Hydrogenotrophic methanogens of the mammalian gut: functionally similar, thermodynamically different. A modelling approach

Rafael Muñoz-Tamayo[1*,¶], Milka Popova[2,¶], Maxence Tillier[2], Diego P. Morgavi [2], Jean-Pierre Morel [3], Gérard Fonty [3], Nicole Morel-Desrosiers[3]

[1]UMR Modélisation Systémique Appliquée aux Ruminants, INRA, AgroParisTech, Université Paris-Saclay, 75005, Paris, France

[2]Institute National de la Recherche Agronomique, UMR1213 Herbivores, Clermont Université, VetAgro Sup, UMR Herbivores, Clermont-Ferrand, France

[3]Université Clermont Auvergne, CNRS, LMGE, F-63000 Clermont-Ferrand, France

Running title: Thermodynamic and kinetic modelling of gut methanogens

*** Correspondence:** Rafael Muñoz-Tamayo, UMR Modélisation Systémique Appliquée aux Ruminants, INRA, AgroParisTech, 16 Rue Claude Bernard, Paris, 75005, France. Tel: 00 33 144081759. E-mail : Rafael.Munoz-Tamayo@inra.fr

¶ These authors contributed equally to this work

Abstract

Methanogenic archaea occupy a unique and functionally important niche in the microbial ecosystem inhabiting the gut of mammals. The purpose of this work was to quantitatively characterize the dynamics of methanogenesis by integrating microbiology, thermodynamics and mathematical modelling. For that, *in vitro* growth experiments were performed with key methanogens from the human and ruminant gut. Additional thermodynamic experiments to quantify the methanogenesis heat flux were performed in an isothermal microcalorimeter. A dynamic model with an energetic-based kinetic function was constructed to describe experimental data. The developed model captures efficiently the dynamics of methanogenesis with concordance correlation coefficients between observations and model predictions of 0.93 for CO_2, 0.99 for H_2 and 0.97 for CH_4. Together, data and model enabled us to quantify species-specific metabolism kinetics and energetic patterns within the group of cytochrome-lacking methanogenic archaea. Using a theoretical exercise, we showed that kinetic information only cannot explain ecological aspects such as microbial coexistence occurring in gut ecosystems. Our results provide new information on the thermodynamics and kinetics of methanogens. This understanding could be useful to (i) construct novel gut models with enhanced prediction capabilities and (ii) devise feed strategies for promoting gut health in mammals and mitigating methane emissions from ruminants.

Introduction

Methanogenic archaea inhabit the gastro-intestinal tract of mammals where they have established syntrophic interactions within the microbial community (1–3) and thus play a critical role in the energy balance. In the human gut microbiota, implication of methanogens in organism homeostasis or diseases is poorly studied, but of growing interest. *Methanobrevibacter smithii* (accounting for 94% of the

methanogen population) and *Methanosphaera stadtmanae* are specifically recognized by the human innate immune system and contribute to the activation of the adaptive immune response (4). Decreased abundance of *M. smithii* was reported in inflammatory bowel diseases patients (5), and it has been shown that methanogens may contribute to obesity (6). In the rumen, the methanogens community is more diverse though still predominated by *Methanobrevibacter* spp., followed by *Methanomicrobium* spp., *Methanobacterium* spp. (7) and *Methanomassillicoccus* spp (8). However, the proportion of these taxa could vary largely, with *Methanomicrobium mobile* and *Methanobacterium formicium* being reported as major methanogens in grazing cattle (9). Though methanogens in the rumen are essential for the optimal functioning of the ecosystem (by providing final electron acceptors), the methane they produce is emitted by the host animal and contributes to global greenhouse gas emissions. Livestock sector is responsible for 14.5 of the anthropogenic greenhouse gas emissions (10). Some *Methanobrevibacter*-related taxa, as *M. smithii, M. gottschalkii, M. milerae and M. thaueri* correlated with higher methane production, whereas *M. ruminantium* was 1.3 fold more abundant in low emitters (11). Methanogens, in general, are phylogenetically and metabolically diverse, but could be separated in two groups based on the presence or absence of cytochromes (12). Most methylotrophic and few hydrogenotrophic methanogens possess membrane-associated cytochrome receiving reducing equivalents from a methanogen specific electronic shuttle, which creates a membrane potential for ATP generation. Major rumen methanogens (13) and the dominant human archaeon, *M. smithii* (14), are hydrogenotrophic without cytochrome. Cytochrome-lacking methanogens exhibit lower growth yields than archaea with cytochromes (*e.g.* aceticlastic methanogens) (12). However, this apparent energetic disadvantage has been counterbalanced by a great adaptation to the environmental conditions (15), and by the establishment of syntrophic interactions with other microbes within the orchestration of the degradation and further fermentation of feed. This syntrophic cooperation centred on the transfer and utilization of hydrogen makes possible anaerobic reactions of substrate conversion to take place close to thermodynamic equilibrium (16,17) (that is with Gibbs free energy change close to zero).

To our knowledge, the impact of thermodynamics on human gut metabolism has been poorly addressed in existing mathematical models (18–21). For the rumen, due to the important role of thermodynamic control on the fermentation, research teams have been motivated in addressing the question of incorporating thermodynamic principles into mathematical models (22–27). Despite these relevant efforts, much work remains to be conducted for attaining a predictive thermodynamic-based model that allows for quantitative assessment of the impact of the thermodynamics on fermentation dynamics. Theoretical frameworks have been developed to allow stoichiometric and energetic balances of microbial growth from the specification of the anabolic and catabolic reactions of microbial metabolism (28,29), and advances have been done to link thermodynamics to kinetics (30–32). These works constitute a solid basis for tackling the thermodynamic modelling of gut metabolism. In this respect, new knowledge on the extent of methanogenesis could help to improve existing gut models. Accordingly, our purpose was to quantitatively characterize the dynamics of hydrogen utilization, methane production, growth and heat flux of three hydrogenotrophic methanogens by integrating microbiology, thermodynamics, and mathematical modelling. We investigated the rate and extent of methanogenesis by performing *in vitro* experiments with three methanogenic species representing major human and ruminant genera: *M. smithii*, *M. ruminantium* and *Methanobacterium formicium.* To interpret and get the most out of the resulting data, a mathematical model with thermodynamic basis was developed to describe the dynamics of the methanogenesis.

Material and Methods

In vitro growth experiments

Archaeal strains and growth media

Archaeal strains used in the study were *Methanobrevibacter ruminantium* DSM 1093, *M. smithii*, and *Methanobacterium formicium*. The growth media was prepared as previously described (33) and

composition is summarized in Table S1 of the Supplementary material. Rumen fluid, that was the main constituent of the culture medium, was sampled through the rumen cannula from a grazing dairy cow prior to the beginning of the experiment. Sampled rumen contents were firstly strained through a monofilament cloth and then centrifuged at 5 000 g for 15 min. Supernatant was autoclaved and then centrifuged again in the same conditions. Clarified rumen fluid was stored at -20°C and centrifuged again after thawing prior to media preparation. Media was boiled to expel dissolved oxygen, a reducing agent (L-cystein) and a redox indicator (resazurin) were added to keep a low redox potential and indicate the oxidative state of the medium respectively. Growth media was distributed in Balch tubes (6 ml per tube), tubes were sealed and sterilized by autoclaving at 121°C for 20 min. Media preparation and distribution was realized under CO_2 flushing to assure anoxic conditions. Oxygen traces from commercial gases were scrubbed using a heated cylinder containing reduced copper (33).

Experimental design and measures

Starter cultures were grown until reaching optical density at 660 nm (OD_{660}) of 0.400 ± 0.030. Optical density was measured on a Jenway spectrophotometer. Then, exactly 0.6 ml were used to inoculate one experimental tube. Commercially prepared high purity H_2/CO_2 (80%/20%) gas mix was added to inoculated tubes by flushing for 1 min at 2.5 Pa. Mean initial OD_{660} and pressure values are summarized in Table S2 of the Supplementary material. Growth kinetics for each strain were followed over 72 h. The experiment was repeated twice. Each kinetics study started with 40 tubes inoculated in the same time. At a given time point, two tubes with similar OD_{660} values were sampled. One of the tubes was used for measuring gas parameters: pressure was measured using a manometer and composition of the gas phase was analysed by gas chromatography on a Micro GC 3000A (Agilent Technologies, France).

Microcalorimetry

111 Microcalorimetric experiments as described by Bricheux et al. (34) were performed to determine the
112 heat flux pattern of each methanogen. Metabolic activity and microbial growth were monitored by
113 using isothermal calorimeters of the heat-conduction type. A TAM III (TA Instruments, France)
114 equipped with two multicalorimeters, each holding six independent microcalorimeters, allowed
115 continuous and simultaneous recording as a function of time of the heat flux produced by 12 samples.
116 The bath temperature was set at 39°C; its long-term stability was better than ± $1x10^{-4}$ °C over 24h.
117 Each microcalorimeter was electrically calibrated. The specific disposable 4 mL microcalorimetric
118 glass ampoules capped with butyl rubber stoppers and sealed with aluminum crimps were filled with
119 1.75 mL of Balch growth media and overpressed with 2.5 Pa of H_2/CO_2 80%/20% gas mixture for 30
120 s. They were sterilized by autoclave and stored at 39°C until the beginning of the microcalorimetric
121 measurements. Actively growing cultures of methanogens (OD_{660} of 0.280±0.030 for *M. smithii*,
122 0.271±0.078 for *M. ruminantium* and 0.142±0.042 for *M. formicium)* were stored at -20°C prior to their
123 injection into the microcalorimetric ampoules. Inoculation was carried out by injecting 0.25 mL of the
124 culture through the septum just before insertion of the overpressed ampoule containing Baltch media
125 into the minicalorimeter. After insertion of the ampoule the sample took about two hours to reach the
126 bath temperature and yield a heat flux equilibrated at zero. Blank experiments were also carried out by
127 inserting ampoules that were not inoculated and, as expected, no heat flux was observed confirming
128 the medium sterility. Each experiment was repeated five times.

129 The heat flux $\left(\frac{dQ}{dt}\right)$, also called thermal power output P, was measured for each methanogen and the
130 blank samples with a precision ≥ 200 nW. The heat flux data of each sample were collected every 5
131 minutes during more than 10 days. The total heat Q was obtained by integrating the overall heat flux–
132 time curve using the TAM Assistant Software and its integrating function (TA Instruments, France).

Classically, the heat flux-time curve for a growing culture starts like the S-shaped biomass curve (a lag phase followed by an exponential growth phase) but differs beyond the growth phase, the heat flux being then modulated by transition periods (34). Heat flux data can be used to infer the microbial growth rate constant. Such inference must be done with caution, since under certain conditions detailed by Braissant et al. (35) lack of correlation occurs between heat flux and microbial growth. The authors suggest that the correlation between isothermal microcalorimetry data and microbiological data (*e.g.*, cell counts) exist at early growth. During the exponential growth phase, microbial growth follows a first-order kinetics defined by the specific growth rate constant μ_c (h^{-1}). Analogously, the heat flux follows an exponential behaviour determined by the parameter μ_c as described by (34,35).

$$\frac{dQ}{dt} = \mu_c \cdot Q \quad (1)$$

The growth rate constant μ_c can be determined by fitting the exponential part of the heat flux-time curve using the fitting function of the TAM Assistant Software. In our case study, careful selection of the exponential phase of heat flux dynamics was performed to provide a reliable estimation of the maximum growth rate constant from calorimetric data.

Mathematical model development

Modelling *in vitro* methanogenesis

The process of *in vitro* methanogenesis is depicted in Figure 1. The H_2/CO_2 mixture in the gas phase diffuses to the liquid phase. The H_2 and CO_2 in the liquid phase are further utilized by the mono-culture of rumen methanogens producing CH_4. Methane in the liquid phase diffuses to the gas phase.

Model construction was inspired on our previous dynamic model of rumen *in vitro* fermentation (36) followed by certain simplifications. Due to the low solubility of hydrogen and methane (37), liquid-gas transfer was only accounted for carbon dioxide. To allow thermodynamic analysis, instead of using the Monod equation in the original formulation, we used in the present work the kinetic rate function proposed by Desmond-Le Quéméner and Bouchez (38). The resulting model is described by the following ordinary differential equations

$$\frac{dx_{\mathrm{H_2}}}{dt} = \mu_{\max} \cdot \exp\left(-\frac{K_s \cdot V_g}{n_{g,\mathrm{H_2}}}\right) \cdot x_{\mathrm{H_2}} - k_d \cdot x_{\mathrm{H_2}} \quad (2)$$

$$\frac{ds_{\mathrm{CO_2}}}{dt} = -\frac{-Y_{\mathrm{CO_2}} \cdot \mu_{\max}}{Y} \cdot \exp\left(-\frac{K_s \cdot V_g}{n_{g,\mathrm{H_2}}}\right) \cdot x_{\mathrm{H_2}} - k_L a \cdot \left(s_{\mathrm{CO_2}} - K_{H,\mathrm{CO_2}} \cdot R \cdot T \cdot n_{g,\mathrm{CO_2}}/V_g\right) \quad (3)$$

$$\frac{dn_{g,\mathrm{H_2}}}{dt} = -\frac{\mu_{\max}}{Y} \cdot \exp\left(-\frac{K_s \cdot V_g}{n_{g,\mathrm{H_2}}}\right) \cdot V_L \cdot x_{\mathrm{H_2}} \quad (4)$$

$$\frac{dn_{g,\mathrm{CO_2}}}{dt} = V_L \cdot k_L a \cdot \left(s_{\mathrm{CO_2}} - K_{H,\mathrm{CO_2}} \cdot R \cdot T \cdot n_{g,\mathrm{CO_2}}/V_g\right) \quad (5)$$

$$\frac{dn_{g,\mathrm{CH_4}}}{dt} = \frac{Y_{\mathrm{CH_4}} \cdot \mu_{\max}}{Y} \cdot \exp\left(-\frac{K_s \cdot V_g}{n_{g,\mathrm{H_2}}}\right) \cdot V_L \cdot x_{\mathrm{H_2}} \quad (6)$$

Where $s_{\mathrm{CO_2}}$ is the concentration (mol/L) of carbon dioxide in the liquid phase and $x_{\mathrm{H_2}}$ is the biomass concentration (mol/L) of hydrogenotrophic methanogens. The number of moles in the gas phase are represented by the variables $n_{g,\mathrm{H_2}}, n_{g,\mathrm{CO_2}}, n_{g,\mathrm{CH_4}}$. The gas phase volume $V_g = 20$ mL and the liquid phase volume $V_L = 6$ mL. Liquid-gas transfer for carbon dioxide is described by a non-equilibria transfer rate which is driven by the gradient of the concentration of the gases in the liquid and gas phase. The transfer rate is determined by the mass transfer coefficient $k_L a$ (h^{-1}) and the Henry's law coefficients $K_{H,\mathrm{CO_2}}$ (M/bar). R (bar·(M · K)$^{-1}$) is the ideal gas law constant and T is the temperature (K). Microbial decay is represented by a first-order kinetic rate with k_d (h^{-1}) the death cell rate constant.

Microbial growth was represented by the rate function proposed by Desmond-Le Quéméner and Bouchez (38) using hydrogen as the limiting reactant

$$\mu = \mu_{\max} \cdot \exp\left(-\frac{K_s \cdot V_g}{n_{g,H_2}}\right) \quad (7)$$

where μ is the growth rate (h^{-1}), μ_{max} (h^{-1}) is the maximum specific growth rate constant and K_s(mol/L) the affinity constant. Equation (7) is derived from energetic principles following Boltzmann statistics and uses the concept of exergy (maximum work available for a microorganism during a chemical transformation). The affinity constant has an energetic interpretation, since it is defined as

$$K_s = \frac{E_M + E_{dis}}{v_{harv} \cdot E_{cat}} \quad (8)$$

where E_{dis} (kJ/mol) and E_M (kJ/mol) are, respectively, the dissipated exergy and stored exergy during growth, E_{cat} (kJ/mol) is the catabolic exergy of one molecule of energy-limiting substrate, and v_{harv} is the volume at which the microbe can harvest the chemical energy in the form of substrate molecules (38). E_{cat} is the absolute value of the Gibbs energy of catabolism ($\Delta G_{r,c}$) when the reaction is exergonic ($\Delta G_{r,c}<0$) or zero otherwise. The stored exergy E_M is calculated from a reaction (destock) representing the situation where the microbe gets the energy by consuming its own biomass. E_M is the absolute value of the Gibbs energy of biomass consuming reaction ($\Delta G_{r,destock}$) when the reaction is exergonic ($\Delta G_{r,destock}<0$) or zero otherwise. Finally, the dissipated exergy E_{dis} is the opposite of the Gibbs energy of the overall metabolic reaction, which is a linear combination of the catabolic and destock reactions. This calculation follows the Gibbs energy dissipation detailed in Kleerebezem and Van Loosdrecht (39).

In our model, the stoichiometry of methanogenesis is represented macroscopically by one catabolic reaction (R_1) for methane production and one anabolic reaction (R_2) for microbial formation. It was

assumed that ammonia is the only nitrogen source for microbial formation. The molecular formula of microbial biomass was assumed to be $C_5H_7O_2N$ (37).

R_1: $4\ H_2 + CO_2 \rightarrow CH_4 + 2\ H_2O$

R_2: $10\ H_2 + 5\ CO_2 + NH_3 \rightarrow C_5H_7O_2N + 8\ H_2O$

In the model, the stoichiometry of the reactions is taken into account *via* the parameters Y, Y_{CO_2}, Y_{CH_4}, which are the yield factors (mol/mol) of microbial biomass, CO_2 and CH_4. The fraction of H_2 utilized for microbial growth (reaction R_2) is defined by the yield factor Y. Now, let f be the fraction of H_2 used for the catabolic reaction R_1. It follows that

$$f = 1 - 10 \cdot Y \tag{9}$$

The yield factors of CO_2 and CH_4 can be expressed as functions of the microbial yield factors:

$$Y_{CO_2} = \left(\frac{1}{4}\right) \cdot f + \left(\frac{5}{10}\right) \cdot (1 - f) \tag{10}$$

$$Y_{CH_4} = \left(\frac{1}{4}\right) \cdot f \tag{11}$$

The model has two physicochemical parameters (k_La, K_{H,CO_2}) and four biological parameters (μ_{max}, K_s, Y, k_d). The initial condition for $s_{CO_2}$is unknown and was also included in the parameter vector for estimation. The Henry's law coefficients are known values calculated at 39°C using the equations provided by Batstone et al. (37).

Theoretical model to study interactions among methanogens

To investigate the ecology of methanogens in the gut ecosystem, we considered a toy model based on the previous model for *in vitro* methanogenesis. Let us consider the following simple model for

representing the consumption of hydrogen by the methanogenic species i under an *in vivo* scenario of continuous flow

$$\frac{dx_{\mathrm{H_2}}}{dt} = \mu_{\max,i} \cdot \exp\left(-\frac{K_{s,i} \cdot V_g}{n_{g,\mathrm{H_2}}}\right) \cdot x_{\mathrm{H_2}} - D_i \cdot x_{\mathrm{H_2}} \quad (12)$$

$$\frac{dn_{g,\mathrm{H_2}}}{dt} = q_{\mathrm{H_2}} - \frac{\mu_{\max,i}}{Y_i} \cdot \exp\left(-\frac{K_{s,i} \cdot V_g}{n_{g,\mathrm{H_2}}}\right) \cdot V_L \cdot x_{\mathrm{H_2}} - b \cdot n_{g,\mathrm{H_2}} \quad (13)$$

where $q_{\mathrm{H_2}}$(mol/h) is the flux of hydrogen produced from the fermentation of carbohydrates. The kinetic parameters are specific to the species i ($x_{\mathrm{H}_{2,i}}$). The parameter D_i (h^{-1}) is the dilution rate of the methanogens and b (h^{-1}) is an output rate constant. Extending the model to n species with a common yield factor Y, the dynamics of hydrogen is given by

$$\frac{dn_{g,\mathrm{H_2}}}{dt} = q_{\mathrm{H_2}} - \frac{V_L}{Y}\sum_{i=1}^{n} \mu_{\max,i} \cdot \exp\left(-\frac{K_{s,i} \cdot V_g}{n_{g,\mathrm{H_2}}}\right) \cdot x_{\mathrm{H}_{2,i}} - b \cdot n_{g,\mathrm{H_2}} \quad (14)$$

where the sub index i indicates the species. In our case study, n = 3.

Parameter identification

Before tackling the numerical estimation of the model parameters, we addressed the question of whether it was theoretically possible to determine uniquely the model parameters given the available measurements from the experimental setup. This question is referred to as structural identifiability (40). Structural identifiability analysis is of particular relevance for model whose parameters are biologically meaningful, since knowing the actual value of the parameter is useful for providing biological insight on the system under study (41). Moreover, in our case, we are interested in finding accurate estimates that can be further used as priors in an extended model describing the *in vivo* system.

We used the freely available software DAISY (42) to assess the structural identifiability of our model. Physical parameters ($k_{\mathrm{L}}\mathrm{a}, K_{\mathrm{H,CO_2}}$) were set to be known. The model was found to be structurally globally identifiable. In practice, however, to facilitate the actual identification of parameters and reduce practical identifiability problems such as high correlation between the parameters (43), some model parameters were fixed to values reported in the literature. The transport coefficient $k_{\mathrm{L}}\mathrm{a}$, the Henry's law coefficient $K_{\mathrm{H,CO_2}}$, and the dead cell rate constant k_{d} were set to be known and were extracted from Batstone et al. (37). Analysis of the data led us to consider the microbial yield factor Y to be the same for all the methanogens. The yield factor was set to be known and its value was taken from Thauer et al. (12) for cytochrome lacking methanogens. Therefore, only the parameters $\mu_{\max}, K_{\mathrm{s}}$ were set to be estimated. To capitalize on the calorimetric data, we further assumed that the specific rate constant (μ_{c}) estimated from the heat flux-time curve is close to the maximal growth rate constant $\mu_{\max}$ of the kinetic function developed by Desmond-Le Quéméner and Bouchez (38). By this, only the affinity constant for each strain was left to be estimated.

The parameter identification of the affinity constant for each methanogen was performed with the IDEAS Matlab® toolbox (44), which is freely available at http://genome.jouy.inra.fr/logiciels/IDEAS. IDEAS uses the maximum likelihood estimator that minimizes the following cost function.

$$J(\boldsymbol{p}) = \sum_{k=1}^{n_{\mathrm{y}}} \frac{n_{\mathrm{t},k}}{2} \ln\left[\sum_{i=1}^{n_{\mathrm{t},k}}\left[y_k\left(t_{i_k}\right) - y_{\mathrm{m}_k}\left(t_{i_k}, \boldsymbol{p}\right)\right]^2\right] \quad (15)$$

where n_{y} is the number of measured variables and $n_{\mathrm{t},k}$the number of observation times for the kth variable y_k, and y_{m_k} is the kth variable predicted by the model. The model output is function of the parameter vector $\boldsymbol{p}$. The measured variables are the number of moles in the gas phase (H_2, CH_4, CO_2). The Lin's concordance correlation coefficient (CCC) (Lin, 1989) was computed to quantify the agreement between the observations and model predictions.

Results

Calorimetric pattern of methanogens

Figure 2 displays a representative isothermal calorimetric curve for each methanogen. The five measured heat flux dynamics of each methanogen were found to follow similar energetic patterns. *M. smithii* and *M. formicium* exhibited a lag phase of a few hours, while *M. ruminantium* was already metabolically active when introduced into the minicalorimeter though several attempts were made to obtain a lag phase by changing storage conditions and thawing the culture just before inoculating the microcalorimetry vials. The pattern of heat flux for all tested methanogens is characterized by one predominant peak which was observed at different times for each methanogen. *M. smithii* exhibited a second metabolic event occurring at 60 h with an increase of heat flux. The same phenomenon is observed for *M. formicium* but at lower intensity at 140 h. One possible explanation for this event is cell lysis (35). At the end of the process, heat flux ceased as result of the end of the metabolic activity. Figure 2 shows a small peak for *M. formicium* at 14 h (a similar peak, but of much smaller size, was observed on the four other curves obtained with this methanogen). *M. smithii* also exhibits a small peak at 7 h that is difficult to visualize at the scale of Figure 2 (the occurrence of this tiny peak was 5 out 5). For *M. ruminantium*, we do not know whether the tiny peak exists since the initial part of the curve is missing. This small peak translates in a metabolic activity that remains to be elucidated.

The total heat (Q_m) produced during the methanogenesis process that took place under the present experimental conditions was, on average, -5.5 J for the three methanogens (for *M. ruminantium*, the missing initial part of the heat flux-time curve was approximately estimated by extrapolating the exponential fit). As we shall see below, this experimental value is consistent with the theoretically expected value.

Estimation of thermodynamic properties

Enthalpies

We defined two macroscopic reactions to represent the catabolism (R1) and anabolism (R2) of the methanogenesis (see Material and Methods). The heat produced during methanogenesis results from the contribution of both catabolic and anabolic reactions. So, first, we calculated the standard enthalpies of the catabolic and anabolic reactions using the standard enthalpies of formation given in Table 1 for the different compounds involved in methanogenesis. The standard enthalpy of the catabolic reaction $\Delta H^{\circ}_{\mathrm{r,c}}$ was calculated as follows

$$\Delta H^{\circ}_{\mathrm{r,c}} = \Delta H^{\circ}_{\mathrm{f,CH_4}} + 2 \cdot \Delta H^{\circ}_{\mathrm{f,H_2O}} - \left(4 \cdot \Delta H^{\circ}_{\mathrm{f,H_2}} + \Delta H^{\circ}_{\mathrm{f,CO_2}}\right) = -252.96 \frac{\mathrm{kJ}}{\mathrm{mol}} \quad (16)$$

A similar equation was used for the calculation of the standard enthalpy of the anabolic reaction $\Delta \mathrm{H}^{\circ}_{\mathrm{r,a}}$

$$\Delta H^{\circ}_{\mathrm{r,a}} = \Delta H^{\circ}_{\mathrm{f,C_5H_7O_2N}} + 8 \cdot \Delta H^{\circ}_{\mathrm{f,H_2O}} - \left(10 \cdot \Delta H^{\circ}_{\mathrm{f,H_2}} + 5 \cdot \Delta H^{\circ}_{\mathrm{f,CO_2}} + \Delta H^{\circ}_{\mathrm{f,NH_3}}\right) = -750.31 \frac{\mathrm{kJ}}{\mathrm{mol}} \quad (17)$$

These results are at 25°C since this is the temperature of the standard enthalpies of formation reported in Table 1. A correction could be made to get results at 39°C but the heat capacities reported by Wagman et al. (45) show that the temperature correction can be neglected. Next, we considered the fact that the heat of a given reaction can be calculated at any state along the reaction pathway via the determination of the reaction coordinate or degree of advancement ε (46). At constant temperature and pressure, the heat produced or consumed by a particular reaction during a given interval can indeed be calculated as follows

$$Q = \int_{\varepsilon_0}^{\varepsilon_{t_f}} \Delta H^{\circ}_{\mathrm{r}} \, \mathrm{d}\varepsilon \quad (18)$$

For our two reactions, at the instant t we have

$$\varepsilon_{\mathrm{c}}(t) = \frac{n_{\mathrm{H_2}}(t) - f \cdot n_{\mathrm{H_{2,0}}}}{-4} \tag{19}$$

$$\varepsilon_{\mathrm{a}}(t) = \frac{n_{\mathrm{H_2}}(t) - (1-f) \cdot n_{\mathrm{H_{2,0}}}}{-10} \tag{20}$$

where $n_{\mathrm{H_2}}(t)$ is the number of moles of hydrogen at the instant t, $n_{\mathrm{H_{2,0}}}$ is the initial number of moles of hydrogen, and f is the fraction of H_2 used for the catabolic reaction. Our calorimetric experiments started with $n_{\mathrm{H_{2,0}}} = 8.83 \cdot 10^{-5}$ mol in all cases. At the final time t_{f}, all the hydrogen was consumed, so that $n_{\mathrm{H_2}}(t_{\mathrm{f}}) = 0$. As indicated in section Parameter Identification, we use the microbial yield factor Y given by Thauer et al. (12) for cytochrome lacking methanogens, that is Y=0.006 which implies that f =0.94. Accordingly, $\varepsilon_{\mathrm{c}} = 2.075 \cdot 10^{-5}$ mol and $\varepsilon_{\mathrm{a}} = 5.30 \cdot 10^{-7}$ mol. It thus follows that the overall heat produced during the methanogenesis process (Q_{m}) can be calculated using the following equation

$$Q_{\mathrm{m}} = Q_{\mathrm{c}} + Q_{\mathrm{a}} = \varepsilon_{\mathrm{c}}(t_{\mathrm{f}}) \cdot \Delta H^{\circ}_{\mathrm{r,c}} + \varepsilon_{\mathrm{a}}(t_{\mathrm{f}}) \cdot \Delta H^{\circ}_{\mathrm{r,a}} \tag{21}$$

where Q_{c} , Q_{a} are the heat produced during catabolism and anabolism respectively. Equation (21) can also be written as

$$Q_{\mathrm{m}} = n_{\mathrm{H_{2,0}}} \left[\frac{(1-10Y)}{4} \,.\, \Delta H^{\circ}_{\mathrm{r,c}} + Y \,.\, \Delta H^{\circ}_{\mathrm{r,a}} \right] \tag{22}$$

Under the experimental conditions, this yields

$$Q_{\mathrm{m}} = Q_{\mathrm{c}} + Q_{\mathrm{a}} = (-5.25) + (-0.40) = -5.65 \text{ J} \tag{23}$$

313 This shows that the anabolic reaction contributes to only 7% of the metabolic heat. It is also interesting
314 to note that there is a very good agreement between the theoretical value calculated above and the
315 overall heat experimentally determined by microcalorimetry (-5.5 J).

316 Since the substrate was totally consumed, the enthalpy of the methanogenesis process per mole (or C-
317 mol) of biomass formed, ΔH_{m}, can be calculated as follows

318 $$\Delta H_{\mathrm{m}} = \frac{Q_{\mathrm{m}}}{n_{\mathrm{biomass}}} = \frac{Q_{\mathrm{m}}}{Y \,.\, n_{\mathrm{H_{2,0}}}} = \frac{(1-10Y)}{4 \,.\, Y} \,.\, \Delta H^{\circ}_{\mathrm{r,c}} + \Delta H^{\circ}_{\mathrm{r,a}} \quad (24)$$

319 which yields

320 $$\Delta H_{\mathrm{m}} = -10658 \frac{\mathrm{kJ}}{\mathrm{mol}} = -2132 \frac{\mathrm{kJ}}{\mathrm{C-mol}} \quad (25)$$

321 **Gibbs energies and entropies**

322 Following a procedure analogous to the one used above for the enthalpies, the standard Gibbs energies
323 of the catabolic ($\Delta G^{\circ}_{\mathrm{r,c}}$) and anabolic ($\Delta G^{\circ}_{\mathrm{r,a}}$) reactions were calculated using the standard Gibbs energies
324 of formation listed in Table 1.

325 $$\Delta G^{\circ}_{\mathrm{r,c}} = \Delta G^{\circ}_{\mathrm{f,CH_4}} + 2 \,.\, \Delta G^{\circ}_{\mathrm{f,H_2O}} - \left(4 \,.\, \Delta G^{\circ}_{\mathrm{f,H_2}} + \Delta G^{\circ}_{\mathrm{f,CO_2}}\right) = -130.62 \ \frac{\mathrm{kJ}}{\mathrm{mol}} \quad (26)$$

326 $$\Delta G^{\circ}_{\mathrm{r,a}} = \Delta G^{\circ}_{\mathrm{f,C_5H_2O_7N}} + 8 \,.\, \Delta G^{\circ}_{\mathrm{f,H_2O}} - \left(10 \,.\, \Delta G^{\circ}_{\mathrm{f,H_2}} + 5 \,.\, \Delta G^{\circ}_{\mathrm{f,CO_2}} + \Delta G^{\circ}_{\mathrm{f,NH_3}}\right) = -248.24 \ \frac{\mathrm{kJ}}{\mathrm{mol}} \quad (27)$$

327 The free energy of the methanogenesis process per mole (or C-mol) of biomass formed, ΔG_{m}, can then
328 obtained from the following equation

329 $$\Delta G_{\mathrm{m}} = \frac{(1-10Y)}{4 \,.\, Y} \,.\, \Delta G^{\circ}_{\mathrm{r,c}} + \Delta G^{\circ}_{\mathrm{r,a}} \quad (28)$$

330

331 which yields

332 $$\Delta G_{\mathrm{m}} = -5364 \ \frac{\mathrm{kJ}}{\mathrm{mol}} = -1073 \ \frac{\mathrm{kJ}}{\mathrm{C-mol}} \quad (29)$$

333 Knowing that, at constant temperature and pressure,

334 $$\Delta G_{\mathrm{m}} = \Delta H_{\mathrm{m}} - T.\Delta S_{\mathrm{m}} \quad (30)$$

335 it follows that the entropic contribution to the methanogenesis process is equal to

336 $$T.\Delta S_{\mathrm{m}} = \Delta H_{\mathrm{m}} - \Delta G_{\mathrm{m}} = -5294 \ \frac{\mathrm{kJ}}{\mathrm{mol}} = -1059 \ \frac{\mathrm{kJ}}{\mathrm{C-mol}} \quad (31)$$

337 which gives, at 39°C, the following value for the entropy of the methanogenesis process per mole (or

338 C-mol) of biomass formed

339 $$\Delta S_{\mathrm{m}} = \frac{(\Delta H_{\mathrm{m}} - \Delta G_{\mathrm{m}})}{(273.15+39)} = -16.96 \ \frac{\mathrm{kJ}}{\mathrm{K^{-1}\ mol}} = -3.40 \ \frac{\mathrm{kJ}}{\mathrm{K^{-1}\ C-mol}} \quad (28)$$

340 In Table 2, the changes in Gibbs energy, enthalpy and entropy observed here during methanogenesis

341 of *M. ruminantium, M. smithii* and *M. formicium* on H_2/CO_2 are compared with values found in the

342 literature for other methanogens grown on different substrates.

343 ## Dynamic description of *in vitro* kinetics

344 The developed mathematical model was calibrated with the experimental data from *in vitro* growth

345 experiments in Balch tubes. Table 3 shows the parameters of the dynamic kinetic model described in

346 Equations 2-6. The reported value of $\mu_{\max}$ for each methanogen corresponds to the average value

347 obtained from five heat flux-time curves. From Table 3, it is concluded that *M. smithii* exhibited the

348 highest growth rate constant, followed by *M. ruminantium* and finally *M. formicium*. In terms of the

affinity constant K_s, while *M. smithii* and *M. ruminantium* have a similar value, the affinity constant for *M. formicium* is lower in one order of magnitude.

Figure 3 displays the dynamics of the compounds in the methanogenesis for the three methanogens. Experimental data are compared against the model responses. Table 4 shows standard statistics for model evaluation. The model captures efficiently the overall dynamics of the methanogenesis. Hydrogen and methane are very well described by the model with concordance correlation coefficients (CCC) of 0.99 and 0.97 respectively. For carbon dioxide, CCC = 0.93.

Figure 4 displays the dynamics of OD_{600} for the methanogens. To infer microbial biomass produced in the anabolic reaction, we used to the data from methane instead of OD_{600} to avoid possible bias due to species-specific absorbance properties of the methanogens. The maximal production of methane among the three microbes was 0.36 mmol for *M. smithii* and 0.33 mmol for *M. ruminantium* and *M. formicium*, which gives an average value of 0.35 ±0.017 mmol (the standard deviation is 3.7% of the mean). This value is fully in agreement with the theoretical value of 0.37 mmoles derived from 1.48 mmol of H_2 (average number of moles at t0) and a yield factor of 0.006. The agreement between the actual methane produced and the theoretical one confirms our hypothesis of considering the same yield factor for all the three methanogens. For our experiment in Balch tubes, approximately 0.009 mmol (1.02 g) of microbial biomass were produced.

Discussion

Our objective in this work was to quantitatively characterize the dynamics of hydrogen utilization, methane production, growth and heat flux of three hydrogenothropic methanogens by integrating microbiology, thermodynamics and mathematical modelling. Our model developments were

instrumental to quantify energetic and kinetic differences between the three methanogens studied, strengthening the potentiality of microcalorimetry as a tool for characterizing the metabolism of microorganisms (34,35,47).

Energetic and kinetic differences between methanogens

Methanogenesis appears as simple reaction with a single limiting substrate (H_2). The microcalorimetry approach we applied revealed that this simplicity is only apparent and that hydrogenotrophic methanogens exhibit energetic and kinetic differences. Methanogenesis is indeed a complex process that could be broken down in several stages. The dominant metabolic phase is represented by one peak that occurs at different times. The magnitude of the peak differs between the methanogens and also the slope of the heat flux trajectories. The return time of the heat flux to the zero baseline was also different. The energetic difference is associated to kinetic differences that translate into specific kinetic parameters, namely affinity constant (K_s) and maximum growth rate constant (μ_{max}). Energetic differences between methanogens has been ascribed by the presence/absence of cytochromes (12). These differences are translated into different yield factors, H_2 thresholds, and doubling times. The kinetic differences revealed in this study for three cytochrome lacking methanogens might indicate that other mechanisms than the presence of cytochromes might play a role on the energetics of methanogenesis. Interestingly, calorimetric experiments show that *M. ruminantium* was metabolically active faster than the other methanogens, suggesting a great adaptation capability for *M. ruminantium* which could be linked to its predominance in the rumen (48).

Looking at the expression of the affinity constant (Equation (8)), and given that we have assumed that all the three methanogens have the same yield factors, it follows that the exergies E_{dis}, E_M, E_{cat} (kJ/mol) are common for all the three species, suggesting that the harvest volume v_{harv} is responsible for the differences between the affinity constants. Note that in the kinetic function developed by

394 Desmond-Le Quéméner and Bouchez (38), the maximum growth rate did not have any dependency on
395 the energetics of the reaction. Our experimental study revealed that μ_{max} is species-specific and reflects
396 the dynamics of the heat flux of the reaction at the exponential phase. Since our study is limited to
397 three species, it is important to conduct further research on other methanogens to validate our findings.

398

399 ## Thermodynamic analysis

400 Regarding the energetic information for different methanogens summarized in Table 2, it is observed
401 that the thermodynamic behaviour of our three methanogens is analogous to that observed for
402 *Methanobacterium thermoautotrophicum* (49) The values reported in Table 3 show indeed that the
403 methanogenesis on H_2/CO_2 is characterized by a large heat production. The growth is highly
404 exothermic, with a ΔH_m value that largely exceeds the values found when other energy substrates are
405 used. The enthalpy change ΔH_m, which is more negative than the Gibbs energy change ΔG_m, largely
406 controls the process. Growth on H_2/CO_2 is also characterized by a negative entropic contribution $T\Delta S_m$
407 which, at first sight, may look surprising since entropy increases in most cases of anaerobic growth
408 (50). However, this can be understood if one remembers that $T\Delta S_m$ corresponds in fact to the balance
409 between the final state and the initial state of the process, that is

410 $$T\Delta S_m = \frac{(1-10Y)}{4Y} T\Delta S_c + T\Delta S_a = \frac{(1-10Y)}{4Y} T(S_{final} - S_{initial})_c + T(S_{final} - S_{initial})_a$$

411 Methanogenesis on H_2/CO_2 is particular because the final state of its catabolic reaction (1 mol CH_4 +
412 2 mol H_2O) involves a smaller number of moles than the initial state (4 mol H_2 + 1 mol CO_2), which
413 results in a significant loss of entropy during the process. For spontaneous growth in such a case, the
414 ΔH_m must not only contribute to the driving force but must also compensate the growth-unfavourable

415 $T\Delta S_m$, which means that ΔH_m must be much more negative than ΔG_m (51). For this reason,
416 methanogenesis on H_2/CO_2, which is accompanied by a considerable decrease of entropy and a large
417 production of heat, has been designed as an entropy-retarded process (52). More generally, (von
418 Stockar and Liu) (51) noticed that when the Gibbs energy of the metabolic process is resolved into its
419 enthalpic and entropic contributions, very different thermodynamic behaviours are observed depending
420 on the growth type: aerobic respiration is clearly enthalpy-driven ($\Delta H_m << 0$ and $T\Delta S_m > 0$) whereas
421 fermentative metabolism is mainly entropy-driven ($\Delta H_m < 0$ and $T\Delta S_m >> 0$) ; methanogenesis on
422 H_2/CO_2 is enthalpy-driven but entropy-retarded ($\Delta H_m << 0$ and $T\Delta S_m < 0$) whereas methanogenesis on
423 acetate is entropy-driven but enthalpy-retarded ($\Delta H_m > 0$ and $T\Delta S_m >> 0$). In the present case, the
424 highly exothermic growth of *M. ruminantium, M. smithii* and *M. formicium* on H_2/CO_2 is largely due
425 to the considerable decrease of entropy during the process: in fact, 50% of the heat produced here
426 serves only to compensate the loss of entropy. A proportion of 80% was found for *M.*
427 *thermoautotrophicum* (49), which results from the fact that their $T\Delta S_m$ and ΔH_m values are,
428 respectively, 2.7 and 1.7 times larger than ours. This difference might be due to the differences of
429 temperature of the studies , namely 39°C in our study vs 60°C in the study by (49).

430

431 **Can we use our results to say something about species coexistence?**

432 The competitive exclusion principle states that coexistence cannot occur between species that occupy
433 the same niche, that is that perform the same function (53), only the most competitive will survive.
434 Recently, by using thermodynamic principles, Großkopf & Soyer (32) demonstrate theoretically that
435 species utilizing the same substrate and producing different compounds can coexist by the action of
436 thermodynamic driving forces. Since in our study, the three methanogens perform the same metabolic
437 reactions, the thermodynamic framework developed Großkopf & Soyer (32) predicts, as the original

exclusion principle (53), the survival of only one species. For continuous culture of microorganisms, it has been demonstrated that at the equilibrium (growth rate equals the dilution rate) with constant dilution rates and substrate input rates, the species that has the lowest limiting substrate concentration wins the competition. From Eq. (12), the number of moles of hydrogen of the species $n^*_{\mathrm{g,H_2},i}$ at the steady state is

$$n^*_{\mathrm{g,H_2},i} = \frac{K_{\mathrm{s},i} \cdot V_{\mathrm{g}}}{\log\left(\mu_{\mathrm{max},i}/D_i\right)}$$

Using the model parameters of Table 3, we studied *in silico* three possible competition scenarios, assuming a constant environment (constant dilution rate D). Two dilution rates were evaluated: D= 0.021 h^{-1} (retention time = 48 h) and D = 0.04 h^{-1} (retention time = 25 h). For D= 0.021 h^{-1}, we obtained that $n^*_{\mathrm{g,H_2,Ms}}$ = 0.36 mmol, $n^*_{\mathrm{g,H_2,Mr}}$ = 0.60 mmol, $n^*_{\mathrm{g,H_2,Mf}}$ = 0.16 mmol where the subindex Ms, Mr, Mf stand for *M. smithii*, *M. ruminantium* and *M. formicium*. From these results, it appears that under a constant environment, *M. formicium* will win the competition. Since $n^*_{\mathrm{g,H_2,Ms}} < n^*_{\mathrm{g,H_2,Mr}}$, *M. ruminantium* will be extinguished before *M. smithii*. For D = 0.04 h^{-1}, we obtained that $n^*_{\mathrm{g,H_2,Ms}}$ = 0.57 mmol, $n^*_{\mathrm{g,H_2,Mr}}$ = 1.27 mmol, $n^*_{\mathrm{g,H_2,Mf}}$ = 0.93 mmol, and thus *M. smithii* wins the competition. In a third hypothetical scenario, with D = 0.04 h^{-1} , we ascribed to *M. ruminantium* better adhesion properties (it is known that both *M. ruminantium* and *M. smithii* genes encode adhesin-like proteins (54,55)). This enhanced adhesion property of *M. ruminantium* was translated mathematically by a factor modulating the microbial residence time as we proposed in our mathematical model of the human colon (18). We then assigned to *M. ruminantium* a 40% of the dilution rate of *M.smithii* and *M. formicium*. We obtained $n^*_{\mathrm{g,H_2,Mr}}$ = 0.50 mmol, and thus *M. ruminantium* wins the competition. To illustrate these aspects, we built a multiple-species model with the three methanogens using Eq. (12) and Eq. (14). The parameter b was set to 0.5 h^{-1} and the hydrogen flux production $q_{\mathrm{H_2}}$ rate was set to

461 0.02 mol/min. Figure 5A displays the dynamics of the three methanogens for the first scenario (D=
462 0.021 h^{-1}). It is observed that at 50 d only *M. formicium* survives. In the rumen context, this result
463 however is not representative of what occurs in reality where the three methanogens coexist (56,57). It
464 is intriguing that in our toy model it is *M. formicium* that wins the competition, bearing in mind that
465 *M. ruminantium* and *M. smithii* are more abundant than *M. formicium* (48,57). Figure 5 shows that
466 selective conditions favour the survival of one species. Similar results can be obtained for the human
467 gut by including the effect of pH on microbial growth (21) and setting the gut pH to select one of the
468 species. On the basis of the competitive exclusion principle, it is thus intriguing that having a very
469 specialized function, methanogens are a diverse group that coexist. In the case of the rumen, our
470 modelling work suggest that in addition to kinetic and thermodynamic factors, other forces contribute
471 to the ecological shaping of the methanogens community in the rumen favouring the microbial
472 diversity. Indeed, methanogenic diversity in the rumen results from multiple factors that include pH
473 sensitivity, the association with rumen fractions (fluid and particulate material), and the endosymbiosis
474 with rumen protozoa (48,57). For the human gut, ecological factors enable methanogens to coexist to
475 competitive environment where hydrogenotrophic microbes (acetogens, methanogenic archaea and
476 sulfate-reducing bacteria) utilize H_2 *via* different pathways (58–60).
477 Finally, mathematical modelling is expected to enhance our understanding of gut ecosystems (61,62).
478 It is then key that in addition to metabolic aspects, mathematical models of gut fermentation incorporate
479 the multiple aspects that shape microbial dynamics to provide accurate predictions and improve insight
480 on gut metabolism dynamics and its potential modulation.
481

482 # Acknowledgements

We are grateful to Dominique Graviou (UMRH, Inra) for her skilled assistance on the *in vitro* growth experiments.

Conflict of interest

No conflict.

References

1. Miller TL, Wolin MJ, Hongxue Z, Bryant MP. Characteristics of methanogens isolated from bovine rumen. Appl Environ Microbiol. 1986;51(1):201–2.

2. Dridi B, Fardeau ML, Ollivier B, Raoult D, Drancourt M. Methanomassiliicoccus luminyensis gen. nov., sp. nov., a methanogenic archaeon isolated from human faeces. Int J Syst Evol Microbiol. 2012;62(8):1902–7.

3. Paul K, Nonoh JO, Mikulski L, Brune A. "Methanoplasmatales," thermoplasmatales-related archaea in termite guts and other environments, are the seventh order of methanogens. Appl Environ Microbiol. 2012;78(23):8245–53.

4. Bang C, Weidenbach K, Gutsmann T, Heine H, Schmitz RA. The intestinal archaea Methanosphaera stadtmanae and Methanobrevibacter smithii activate human dendritic cells. PLoS One. 2014;9(6).

5. Ghavami SB, Rostami E, Sephay AA, Shahrokh S, Balaii H, Aghdaei HA, et al. Alterations of the human gut Methanobrevibacter smithii as a biomarker for inflammatory bowel diseases. Microb Pathog. 2018;117:285–9.

6. Mathur R, Barlow GM. Obesity and the microbiome. Vol. 9, Expert Review of

Gastroenterology and Hepatology. 2015. p. 1087–99.

7. Hook SE, Wright A-DG, McBride BW. Methanogens: methane producers of the rumen and mitigation strategies. Archaea 2010:945785.

8. Poulsen M, Schwab C, Jensen BB, Engberg RM, Spang A, Canibe N, et al. Methylotrophic methanogenic Thermoplasmata implicated in reduced methane emissions from bovine rumen. Nat Commun. 2013;4:1428.

9. Jarvis GN, Strömpl C, Burgess DM, Skillman LC, Moore ERB, Joblin KN. Isolation and identification of ruminal methanogens from grazing cattle. Curr Microbiol. 2000;40(5):327–32.

10. Gerber P, Steinfeld H, Henderson B, Mottet A, Opio C, Dijkman J, et al. Tackling Climate Change through Livestock. Food and Agriculture Organization. 2013; 15-21.

11. King EE, Smith RP, St-Pierre B, Wright ADG. Differences in the rumen methanogen populations of lactating Jersey and holstein dairy cows under the same diet regimen. Appl Environ Microbiol. 2011;

12. Thauer RK, Kaster AK, Seedorf H, Buckel W, Hedderich R. Methanogenic archaea: Ecologically relevant differences in energy conservation. Vol. 6, Nature Reviews Microbiology. 2008. p. 579–91.

13. Friedman N, Jami E, Mizrahi I. Compositional and functional dynamics of the bovine rumen methanogenic community across different developmental stages. Environ Microbiol. 2017;19(8):3365–73.

14. Hansen EE, Lozupone CA, Rey FE, Wu M, Guruge JL, Narra A, et al. Pan-genome of the

524 dominant human gut-associated archaeon, Methanobrevibacter smithii, studied in twins. Proc
525 Natl Acad Sci [Internet]. 2011;108(Supplement_1):4599–606.

526 15. Morgavi DP, Forano E, Martin C, Newbold CJ. Microbial ecosystem and methanogenesis in
527 ruminants. Animal [Internet]. 2010 Jul [cited 2014 Nov 28];4(7):1024–36.

528 16. Jackson BE, McInerney MJ. Anaerobic microbial metabolism can proceed close to
529 thermodynamic limits. Nature. 2002;415(6870):454–6.

530 17. González-Cabaleiro R, Lema JM, Rodríguez J, Kleerebezem R. Linking thermodynamics and
531 kinetics to assess pathway reversibility in anaerobic bioprocesses. Energy Environ Sci. 2013;
532 6(12):3780.

533 18. Muñoz-Tamayo R, Laroche B, Walter E, Doré J, Leclerc M. Mathematical modelling of
534 carbohydrate degradation by human colonic microbiota. J Theor Biol. 2010; 266(1):189–201.

535 19. Van Wey AS, Lovatt SJ, Roy NC, Shorten PR. Determination of potential metabolic pathways
536 of human intestinal bacteria by modeling growth kinetics from cross-feeding dynamics. Food
537 Res Int. 2016;88:207–16.

538 20. Shoaie S, Ghaffari P, Kovatcheva-Datchary P, Mardinoglu A, Sen P, Pujos-Guillot E, et al.
539 Quantifying Diet-Induced Metabolic Changes of the Human Gut Microbiome. Cell Metab.
540 2015;22(2):320–31.

541 21. Kettle H, Louis P, Holtrop G, Duncan SH, Flint HJ. Modelling the emergent dynamics and
542 major metabolites of the human colonic microbiota. Env Microbiol. 2014; 17(5):1615-30.

543 22. Janssen PH. Influence of hydrogen on rumen methane formation and fermentation balances
544 through microbial growth kinetics and fermentation thermodynamics. Anim Feed Sci Technol.

2010; 160(1–2):1–22.

23. Kohn R a, Boston RC. The Role of Thermodynamics in Controlling Rumen Metabolism. Model Nutr Util Farm Anim. 2000;11–24.

24. Offner A, Sauvant D. Thermodynamic modeling of ruminal fermentations. Anim Res. 2006;55(5):343–65.

25. Ungerfeld EM. A theoretical comparison between two ruminal electron sinks. Front Microbiol. 2013;4.

26. Van Lingen HJ, Plugge CM, Fadel JG, Kebreab E, Bannink A, Dijkstra J. Thermodynamic driving force of hydrogen on rumen microbial metabolism: A theoretical investigation. PLoS One. 2016;11(10).

27. Ghimire S, Gregorini P, Hanigan MD. Evaluation of predictions of volatile fatty acid production rates by the Molly cow model. J Dairy Sci. 2014;97(1):354–62.

28. Heijnen JJ, Van Dijken JP. In search of a thermodynamic description of biomass yields for the chemotrophic growth of microorganisms. Biotechnol Bioeng. 1992;39(8):833–58.

29. Kleerebezem R, Van Loosdrecht MCM. A Generalized Method for Thermodynamic State Analysis of Environmental Systems. Crit Rev Environ Sci Technol. 2010;40(1):1–54.

30. Hoh CY, Cord-Ruwisch R. A practical kinetic model that considers endproduct inhibition in anaerobic digestion processes by including the equilibrium constant. Biotechnol Bioeng. 1996;51(5):597–604.

31. Desmond-Le Quemener E, Bouchez T. A thermodynamic theory of microbial growth. Isme J. 2014;8(8):1747–51.

566 32. Großkopf T, Soyer OS. Microbial diversity arising from thermodynamic constraints. ISME J.
567 2016;10(11):2725–33.

568 33. Wolfe RS. Techniques for cultivating methanogens. Methods Enzymol. 2011;494:1–22.

569 34. Bricheux G, Bonnet JL, Bohatier J, Morel JP, Morel-Desrosiers N. Microcalorimetry: a
570 powerful and original tool for tracking the toxicity of a xenobiotic on Tetrahymena pyriformis.
571 Ecotoxicol Env Saf. 2013;98:88–94.

572 35. Braissant O, Bonkat G, Wirz D, Bachmann A. Microbial growth and isothermal
573 microcalorimetry: Growth models and their application to microcalorimetric data.
574 Thermochim Acta. 2013;555:64–71.

575 36. Muñoz-Tamayo R, Giger-Reverdin S, Sauvant D. Mechanistic modelling of in vitro
576 fermentation and methane production by rumen microbiota. Anim Feed Sci Technol.
577 2016;220.

578 37. Batstone DJ, Keller J, Angelidaki I, Kalyuzhnyi S V, Pavlostathis SG, Rozzi A, et al.
579 Anaerobic Digestion Model No.1 (ADM1). IWA Publishing, London; 2002. 65-73 p.

580 38. Desmond-Le Quéméner E, Bouchez T. A thermodynamic theory of microbial growth. ISME J.
581 2014;8(8):1747–51.

582 39. Kleerebezem R, Van Loosdrecht MCM. A Generalized Method for Thermodynamic State
583 Analysis of Environmental Systems. Crit Rev Environ Sci Technol [Internet]. 2010;40(1):1–
584 54.

585 40. Walter E, Pronzato L. Identification of Parametric Models from Experimental Data. Springer,
586 London; 1997.

587 41. Muñoz-Tamayo R, Puillet L, Daniel JB, Sauvant D, Martin O, Taghipoor M, et al. Review: To
588 be or not to be an identifiable model. Is this a relevant question in animal science modelling?
589 Animal. 2018;12(4):701–12.

590 42. Bellu G, Saccomani MP, Audoly S, D'Angiò L. DAISY: A new software tool to test global
591 identifiability of biological and physiological systems. Comput Methods Programs Biomed.
592 2007;88(1):52–61.

593 43. Vanrolleghem PA, Vandaele M, Dochain D. Practical Identifiability of a Biokinetic Model of
594 Activated-Sludge Respiration. Water Res. 1995;29(11):2561–70.

595 44. Muñoz-Tamayo R, Laroche B, Leclerc M, Walter E. IDEAS: A parameter identification
596 toolbox with symbolic analysis of uncertainty and its application to biological modelling. In:
597 IFAC Proceedings Volumes (IFAC-PapersOnline). 2009.

598 45. Wagman DD, Evans WH, Parker VB, Schumm RH, Halow I, Bailey SM, et al. The Nbs
599 Tables of Chemical Thermodynamic Properties - Selected Values for Inorganic and C-1 and
600 C-2 Organic-Substances in Si Units. J Phys Chem Ref Data. 1982;11:S2.

601 46. Prigogine I, Defay R. Traité de thermodynamique, conformément aux méthodes de Gibbs et
602 De Donder. Éditions Desoer. Liège; 1950.

603 47. Ruiz T, Bec A, Danger M, Koussoroplis A, Aguer J, Morel J, et al. A microcalorimetric
604 approach for investigating stoichiometric constraints on the standard metabolic rate of a small
605 invertebrate. Ecol Lett. 2018;21:1714–22.

606 48. Janssen PH, Kirs M. Structure of the archaeal community of the rumen. Appl Environ
607 Microbiol. 2008;74(12):3619–25.

608 49. Schill NA, Liu JS, von Stockar U. Thermodynamic analysis of growth of Methanobacterium
609 thermoautotrophicum. Biotechnol Bioeng. 1999;64(1):74–81.

610 50. von Stockar U, Larsson C, Marison IW. Calorimetry and energetic efficiencies in aerobic and
611 anaerobic microbial growth. Pure Appl Chem. 1993;65(9):1889–92.

612 51. Von Stockar U, Liu JS. Does microbial life always feed on negative entropy? Thermodynamic
613 analysis of microbial growth. Biochim Biophys Acta - Bioenerg. 1999;1412(3):191–211.

614 52. Schill N, Liu J-S, von Stockar U. Thermodynamic analysis of growth of methanobacterium
615 thermoautotrophicum. Biotechnol Bioeng. 1999;64(1):74–81.

616 53. Hardin G. The Competitive Exclusion Principle. Science. 1960;131(3409):1292–7.

617 54. Ng F, Kittelmann S, Patchett ML, Attwood GT, Janssen PH, Rakonjac J, et al. An adhesin
618 from hydrogen-utilizing rumen methanogen Methanobrevibacter ruminantium M1 binds a
619 broad range of hydrogen-producing microorganisms. Env Microbiol. 2016;18(9):3010–21.

620 55. Samuel BS, Hansen EE, Manchester JK, Coutinho PM, Henrissat B, Fulton R, et al. Genomic
621 and metabolic adaptations of Methanobrevibacter smithii to the human gut. Proc Natl Acad
622 Sci. 2007;104(25):10643–8.

623 56. Kelly WJ, Leahy SC, Li D, Perry R, Lambie SC, Attwood GT, et al. The complete genome
624 sequence of the rumen methanogen Methanobacterium formicicum BRM9. Stand Genomic
625 Sci. 2014;9(1):1–8.

626 57. Carberry CA, Waters SM, Kenny DA, Creevey CJ. Rumen methanogenic genotypes differ in
627 abundance according to host residual feed intake phenotype and diet type. Appl Env
628 Microbiol. 2014;80(2):586–94.

629 58. Bernalier A, Lelait M, Rochet V, Grivet JP, Gibson GR, Durand M. Acetogenesis from H2 and
630 CO2 by methane- and non-methane-producing human colonic bacterial communities. FEMS
631 Microbiol Ecol. 1996;19(3):193–202.

632 59. Nava GM, Carbonero F, Croix JA, Greenberg E, Gaskins HR. Abundance and diversity of
633 mucosa-associated hydrogenotrophic microbes in the healthy human colon. ISME J.
634 2012;6(1):57–70.

635 60. Flint HJ, Duncan SH, Scott KP. Minireview Interactions and competition within the microbial
636 community of the human colon : links between diet and health. Environ Microbiol. 2007;

637 61. Widder S, Allen RJ, Pfeiffer T, Curtis TP, Wiuf C, Sloan WT, et al. Challenges in microbial
638 ecology: Building predictive understanding of community function and dynamics. ISME J.
639 2016;10(11):2557–68.

640 62. Huws SA, Creevey, Christopher J. Oyama LB, Mizrahi I, Denman SE, Popova M, Muñoz-
641 Tamayo, Rafael Forano E, et al. Addressing global ruminant agricultural challenges through
642 understanding the rumen microbiome: Past, present and future. Front Microbiol. 2018;9:2161.

643 63. Liu JS, Marison IW, von Stockar U. Microbial growth by a net heat up-take: A calorimetric
644 and thermodynamic study on acetotrophic methanogenesis by Methanosarcina barkeri.
645 Biotechnol Bioeng. 2001;75(2):170–80.

646

647

648

649

650 **Table 1** Standard enthalpies ($\Delta H_f°$) and Gibbs energies ($\Delta G_f°$) of formation at 25°C of compounds
651 involved in hydrogenotrophic methanogenesis. Values were extracted from Wagman et al (45), with
652 the exception of the microbial biomass that was calculated from values for *Methanosarcina barkeri*
653 reported by Liu et al. (63)

Compound (phase)	$\Delta H_f°$ (kJ/mol)	$\Delta G_f°$ (kJ/mol)
H_20 (l)	-285.830	-237.129
H_2 (g)	0	0
CO_2 (g)	-393.509	-394.359
CH_4 (g)	-74.81	-50.72
NH_3 (aq)	-80.29	-26.50
$C_5H_7O_2N$	-511.50*	-349.50*

654 * These values are five times the values reported by Liu et al. (63) since the biomass formula we used
655 has five carbon molecules, while the biomass formula used by Liu et al. has one carbon.

656

657

658

659 **Table 2** Gibbs energies, enthalpies and entropies of metabolic processes involving some methanogens

660 growing on different energy sources

Microorganism	Energy substrate	Growth conditions	ΔG_m kJ / C-mol	ΔH_m kJ / C-mol	$T\Delta S_m$ kJ / K^{-1} C-mol	Driving force	Reference
M. ruminantium, *M. smithii*, *M. formicium*	H_2/CO_2	anaerobic	-1073	-2139	-1066	Enthalpy-driven but Entropy-retarded	this work
M. thermo-autotrophicum	H_2/CO_2	anaerobic	-802	-3730	-2928	Enthalpy-driven but Entropy-retarded	(52)
M. formicium	formate	anaerobic	-880	-613	+267	Enthalpy-driven	(28)
M. barkeri	methanol	anaerobic	-570	-420	+150	Enthalpy-driven	(28)
M. barkeri	acetate	anaerobic	-366	+145	+511	Entropy-driven but enthalpy-retarded	(63)

661

662

663

664 **Table 3 Parameters of the model of *in vitro* methanogenesis. The value reported**

665 **μ_{max} for each methanogen is the mean value obtained from five heat flux-time curves**

Parameter	Definition	Value		
$k_L a$ (h^{-1})	Liquid–gas transfer constant	8.33		
K_{H,CO_2} (M/bar)	Henry's law coefficient of carbon dioxide	0.0246		
k_d (h^{-1})	Death cell rate constant	8.33×10^{-4}		
Y (mol biomass /mol H_2)	Microbial biomass yield factor	0.006		
		M. smithii	*M. ruminantium*	*M. formicium*
K_s (mol/L)	Affinity constant	0.032	0.037	0.007
μ_{max} (h^{-1})	Maximum specific growth rate constant	0.12	0.07	0.046

666

667

668

669

670 **Table 4 Statistical indicators for model evaluation**

Component	CCC^{*}	r^2	$CV_{RMSE}{}^{**}$
Hydrogen	0.99	0.97	14
Methane	0.97	0.95	17
Carbon dioxide	0.93	0.86	6

671 * CCC: Lin's concordance correlation coefficient.

672 ** CV_{RMSE}: coefficient of variation of the root mean squared error.

673

674

675

676

677

678

679

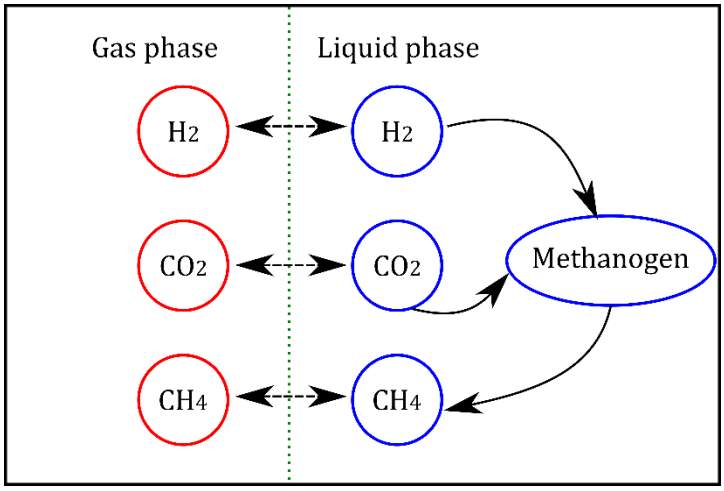

680 **Figure 1** Schematics of the *in vitro* methanogenesis process. Double arrows represent fluxes due to

681 liquid-gas transfer, simple arrows represent metabolic fluxes.

682

683

684

685

686

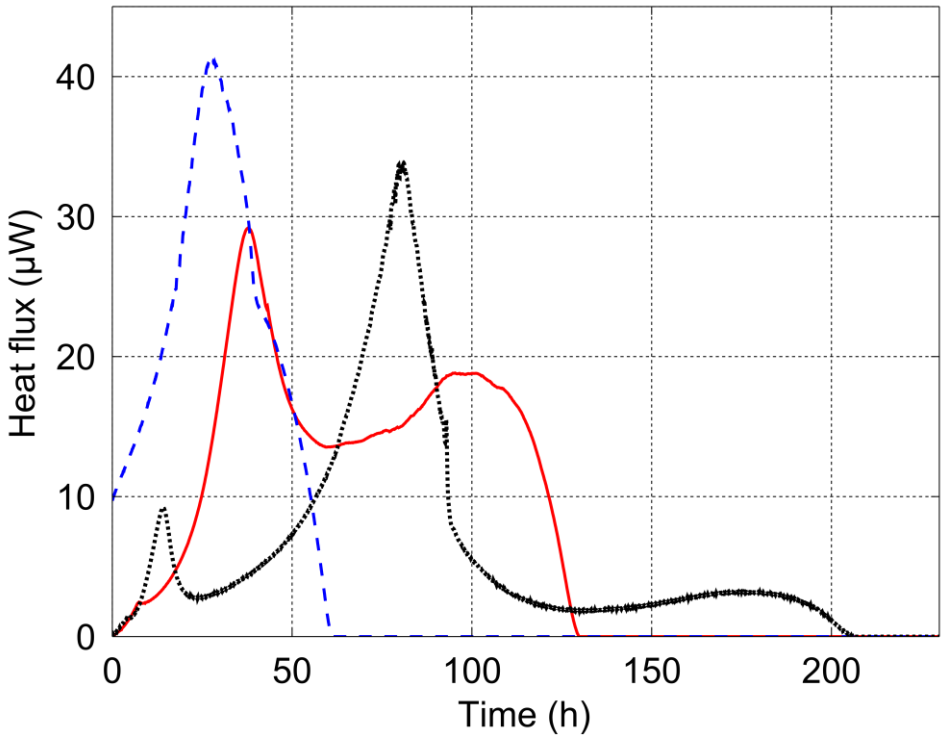

687

688 **Figure 2** Example of isothermal calorimetric curves for *M. ruminantium* (dashed blue line), *M. smithii*
689 (solid red line) and *M. formicium* (dotted black line). The dominant metabolic phase is represented by
690 one peak. The magnitude of the peak differs between the methanogens and also the slope of the heat
691 flux trajectories. The return of the heat flux to the zero baseline also differs between the three
692 methanogens.

693

694

695

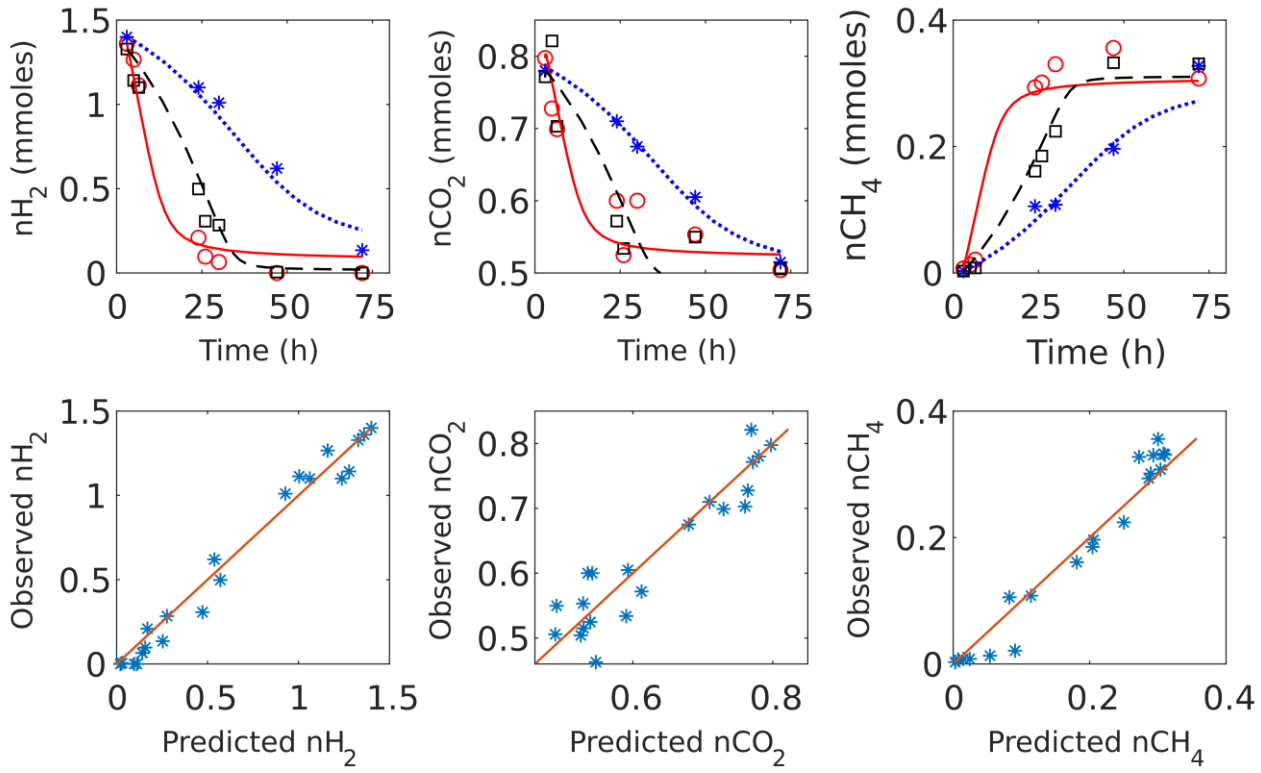

696

697 **Figure 3** Top plots: dynamics of methanogenesis by *M. ruminantium* (*), *M. smithii* (o) and *M.*

698 *formicium* (□). Experimental data (*,o,□) are compared against model predicted responses: dotted blue

699 lines (*M. ruminantium*), solid red lines (*M. smithii*) and dashed black lines (*M. formicium*). Bottom

700 plots: summary of observed vs predicted variables**.** The solid red line is the isocline.

701

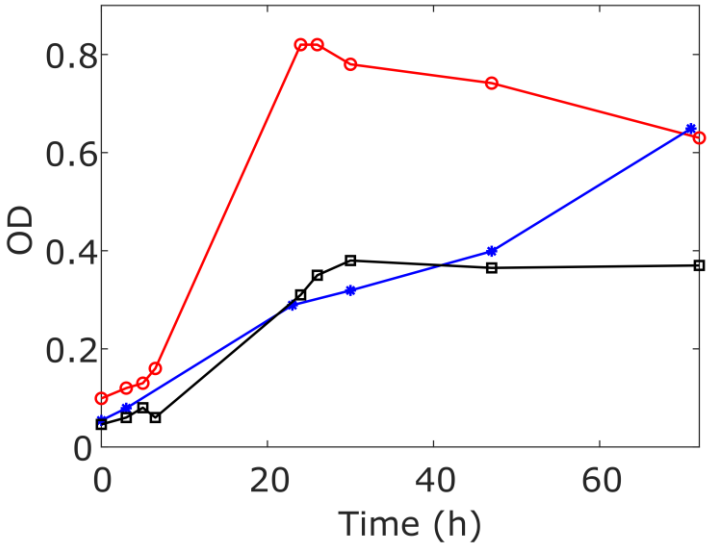

Figure 4 Dynamics of the optical density (OD_{600}) for *M. ruminantium* (*), *M. smithii* (o) and *M. formicium* (□). Maximal values differ between the three methanogens.

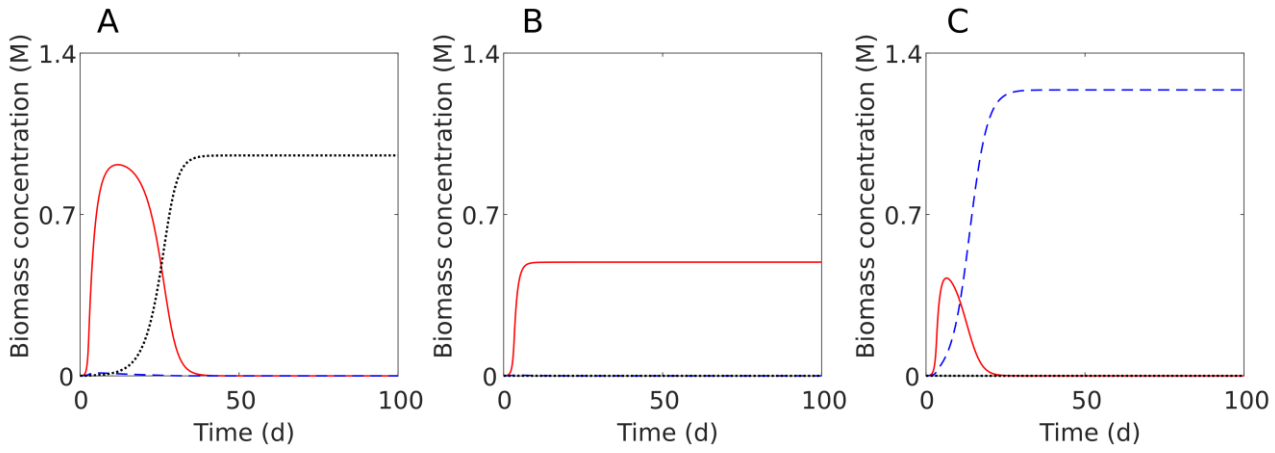

Figure 5 Possible competition scenarios between *M. ruminantium* (blue dashed line), *M. smithii* (red solid line) and *M. formicium* (black dotted line) in a hypothetical constant environment. A. At constant dilution rate of 0.021 h^{-1}, *M. formicium* displaces the other two methanogens. B. With a constant dilution rate of 0.04 h^{-1}, *M. smithii* wins the competition. C. Assuming that, thanks to its adhesion properties, *M. ruminantium* has a 40% lower dilution rate than that of the other methanogens, it wins the competition. At constant environmental conditions, only one species wins and displaces the other methanogens.

Supplementary Material

Table S1 Methanogens growth media composition.

Composition per 100 ml	Amount
Clarified rumen fluid	30 ml
Dipotassium phosphate (K_2HPO_4) 0.06% (w/v)	5 ml
Balch Mineral solution [1]	5 ml
Tryptone	0.2 g
Yeast extract	0.2 g
Balch oligo-elements solution [2]	1 ml
Balch vitamin solution[3]	1 ml
Resazurin 0.1%	1 ml
Ammonium chloride	0.05 g
Sodium acetate	0.25 g
Sodium formate	0.25 g
Sodium carbonate	0.5g
L-cystein HCl	0.4g
Distilled water	qs 100 ml

[1] $KH_2PO_4.2H_2O$ (0.6g), $(NH_4)_2SO_4$ (0.6g), NaCl (1.2g), $MgSO_4.7H_2O$ (0.12g), $CaCl_2.2H_2O$ (0.12g), distilled water qs 100 ml

[2] Nitrilotriacetic acid (0.15 g), $MgSO_4.7H_2O$ (0.3g), $MnSO_4.2H_2O$ (0.05g), NaCl (0.1g), $FeSO_4.7H_2O$ (0.01g), $CoSO_4$ (0.01g), $CaCl_2.2H_2O$ (0.01g), $ZnSO_4.2H_2O$ (0.01g), $CuSO_4.5H_2O$ (0.001g), $AlK(SO_4)_2$ (0.001g), H_3BO_3 (0.001g), $NaMoO_4.2H_2O$ (0.001g), $NiCl.6H_2O$ (0.01g), Na_2SeO_3 (0.001g), distilled water qs 100 ml

[3] Biotine (0.2 mg), PABA (0.5 mg), Riboflavine (0.5 mg), Pantothenic acid (0.5 mg), Sodium ascorbate (0.5 mg), Folic acid (0.2 mg), Niacin (0.5 mg), Pyridoxine (0.10 mg), thiamine (0.05 mg), Vitamin B12 0.1mg/ml (0.1 ml), lipoic acid (0.5 mg), Choline chloride (0.5 mg), Inositol (0.5 mg), Nicotinamide (0.5 mg), Pyridoxal (0.5mg), distilled water qs 100 ml

742 **Table S2**

743 Inoculation conditions

744

Strain	*Methanobrevibacter ruminantium*	*Methanobrevibacter smithii*	*Methanobacterium formicium*	Effect of the experiment
Initial OD	0.054	0.099	0.046	<0.001
Initial pressure (mbar)	2996	2927	2910	0.0025

745